*Journal of Sound and Vibration* (1997) **199**(4), 531–558

# DYNAMIC MODELLING OF RAILWAY TRACK: A PERIODIC MODEL BASED ON A GENERALIZED BEAM FORMULATION

L. Gry and C. Gontier

*Ecole Centrale de Paris, Laboratoire de Mécanique des Sols & Structures & Matériaux, Chatenay-Malabry, France*

(*Received* 7 *February* 1994, *and in final form* 17 *January* 1995)

Dynamic modelling of railway track is a vital step in view of traffic noise reduction. Considering the track as a periodic structure, the classical properties and methods associated with one-dimensional periodic structures are recalled, then applied to the problem within the framework of the Euler–Bernouilli and Timoshenko beam theories. These methods turn out to be insufficient when compared with experimental data, especially concerning the lateral receptance spectrum. Therefore, an extended beam model is developed, essentially based on the notion of generalized cross-section displacements. Finally, the application of this theory to railway track results in a significant improvement in the computed spectrum, and suggests directions for further investigations.



## 1. INTRODUCTION

### 1.1. ROLLING NOISE REDUCTION

Today, the problem of noise reduction of railway track is attracting growing interest in many industrial countries. At the current commercial speeds of modern trains—about 300 km/h—it is generally assumed that about 70% of the traffic noise originates from the wheel–track couple, the rest being generated by aerodynamic effects. Because of the predominance of the former factor, the efforts of engineers concerned with track noise reduction are essentially devoted to it.

Concerning the wheel–rail noise, rough estimations show that half originates from track vibration, while the other half is produced by wheel deformation. To reach an acceptable decrease in global noise, both components are analyzed simultaneously by engineers. Actually, of these two aspects, track vibration appears to be the most difficult to model, because the phenomenon is complex in itself. It has generally been found that a direct finite element (F.E.) analysis of the track structure does not provide sufficiently accurate results for the dynamics. For this reason an important effort has been devoted in the past to a theoretical investigation of the problem. Several approaches are now available. The present paper represents a continuation of this research, in order to improve the physical representativeness of the models.

### 1.2. RAILWAY TRACK MODELLING

There are several difficulties involved in dynamic track modelling. The rail by itself has a complex geometry (see Figure 1) which presents most of the coupling phenomena that exist in classical beam theory; i.e., torsional, bending and shearing deformations. Another

0022–460X/97/040531 + 28 $25.00/0/sv950671 

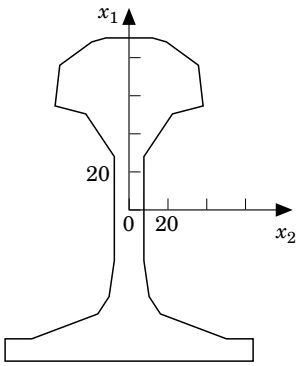


Figure 1. The cross-section of the rail (dimensions in mm).

difficulty is related to the presence of repetitive supports—sleepers, pads and ballast—especially as the dynamic characteristics of those elements are generally known with poor accuracy. Finally, it is suspected today that the deformation models of classical beam theory may not be appropriate, especially in the high frequency range, to provide a satisfactory representation of rail vibration.

In short, two different paths have been followed by previous researchers who have investigated the problem. In the first approach, the representation of the track has been based on infinite beam models; while in the second approach the model has been derived from the theory of periodic structures.

### 1.3. THE INFINITE BEAM MODELS

The rail is considered as an infinite beam, and its dynamic behaviour can be studied by the classical methods of wave propagation analysis. In this approach the supports can either be ignored or included in the model in the form of a continuous multi-layer foundation, defined by a set of mass, stiffness and damping densities. After the work of Remington [1] and Grassie [2], both based on the Euler–Bernouilli beam model, an extensive investigation was carried out by Thompson [3], who used a F.E. approach to study a 2·08 m rail length representing the infinite beam. With computation of the normal modes of the rail, Thompson showed that at low frequencies—below 1500 Hz—the vibration modes of the structure could be recognized as the classical deformation modes of beam theory: i.e., bending, torsional and longitudinal modes. On the other hand, he found that, when increasing the frequency above 1500 Hz, the mode shapes changed progressively so as to incorporate more and more in-plane deformation of the cross-section. For instance, at high frequencies, bending modes progressively incorporate foot flapping effects, while the torsional mode incorporates more and more web bending effects.

### 1.4. THE PERIODIC STRUCTURE MODELS

The second approach is based on the theory of wave propagation in periodic structures. The general problem has received great attention from various authors in the past. Physicists were the first to work in this field, applying it to wave propagation problems in crystalline structures [4]. Ultimately, their work was generally oriented towards two- or three-dimensional structures.

Various applications to one-dimensional structures such as stiffened plates [5, 6], skin-rib structures [7, 8], truss beam structures [9–11], multi-supported beams [12, 13] and other

periodic structures have furnished researchers with many opportunities for investigation in the past. In this field, Mead's contribution deserves special attention. In his early papers [12–15] he clarified the stop-band/pass-band phenomenon, and investigated the relations between the pass-band frontier frequencies and the single element eigenfrequencies. Then he thoroughly studied the question of inter-element energy transfers, and finally proposed a clear analysis of the relations between the pass-bands of the infinite system and the natural frequencies of finite systems [8].

Another contribution, which brought a different insight into the problem, has come in recent years from Pierre. He has made systematic use of the inter-element transfer matrix [11], which was found later to present real advantages in terms of generality and practicality. The present paper is essentially based on this fundamental notion. In recent papers, he has widely investigated the question of quasi-periodicity [10, 11], using probabilistic theories, and thoroughly discussed the localizing effect of near-periodicity [16, 17].

Heckl [19] has investigated applications to track vibration while allowing for the presence of discrete supports, and then Thompson [3] adapted the method to a F.E. approach. While including a double-layer continuous foundation, he reached results that essentially confirmed the conclusions of the first approach, and provided additional useful data concerning the role of certain parameters, such as support characteristics and damping coefficients.

### 1.5. THE NEED FOR FURTHER INVESTIGATION OF THE PROBLEM

The drawbacks of the previous methods are a consequence of their inherent nature. The pure analytical method is naturally restricted to the classical models of beam deformation, and so cannot take into account all of the deformation patterns that are expected to be found in the present case. Moreover, the classical coupling effects of the beam theory, such as shearing and torsional interactions in relation to the location of the shear center, are difficult to include in the wave equation, whereas they are quite relevant to the specific geometry of the rail case.

Even with the improvement of the periodic structure theory, the F.E. approach leads naturally to heavy computations because of the necessary longitudinal discretization. Moreover, our practical experience in the field has revealed that, due to the presence of near-field waves of very short wavelength, numerical difficulties can hardly be avoided with this method.

The purpose of the present paper is to develop a generalized approach to the problem, that will remain within the framework of periodic structure theory, while retaining the advantages of the analytical method and some of the advantages of the F.E. method. As we will see, the advantages of the analytical method are obtained by using a Fourier decomposition in the longitudinal direction, while the advantages of the F.E. method are drawn from a discretization of the cross-sectional displacements.

So far, our method could be defined as a 'finite strip method''. However, due to the F.E. discretization of the cross-section, we would be led once more to matrix equations of large dimensions, involving the same difficulties as above. For this reason, another concept has been introduced in order to reduce the spatial dimensions of the displacement field. On the assumption that the deformation of the cross-section can be approximately described from a reduced number of deformation patterns called ''cross-section modes'', the wave equations are developed on this reduced basis, and so the periodic analysis is finally made using a small sized matrix equation.

Although the final purpose of the method is to provide a precise description of the vibrational behaviour of a track, by including as many ''cross-section modes'' as necessary

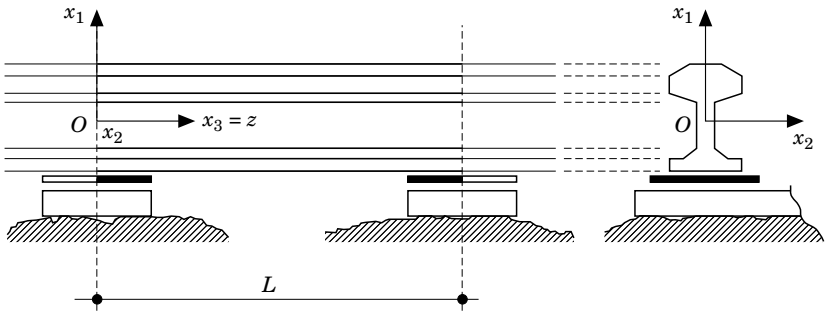


Figure 2. The definition of the periodic track element and reference frame.

in the model, the aim of this first paper will not be so ambitious. First, we intend to develop a mathematical formulation of what we call our hybrid approach, and then show its equivalence with the previous methods used in the literature. This will be the content of sections 2 and 3. After a short review of the theory of periodic structures in section 2, the direct application of this theory to the track structure, within the framework of the Euler–Bernouilli beam model, will be presented in section 3. At this point the insufficiency of the Euler–Bernouilli model, even with the added improvement of the Timoshenko factors, will be established. The truly new concepts of our method will be introduced in section 4, with the notion of "cross-section modes", and the elasto-dynamic equations implied by this concept will be developed. Finally, the power of the method will be demonstrated by means of an example including only two additional modes.

## 2. THE ONE-DIMENSIONAL PERIODIC MODEL

In this section, some useful notions and formulas of the one-dimensional periodic structure theory will be recalled. Although these notions have a quite general value, for the sake of brevity they will be presented in the framework of the railway track application.

### 2.1. TRANSFER MATRIX OF A PERIODIC STRUCTURE

The transfer matrix method was chosen since it leads to a very clear presentation of wave propagation phenomena in periodic structures. This section is devoted to the derivation of the track span transfer matrix. The developments refer to Figures 1 and 2, which describe the structure and the co-ordinate system. Note that the longitudinal co-ordinate will be indifferently labelled $z$ or $x_3$ throughout the text.

In this approach, a vector $\mathbf{U}$ of independent variables must be chosen and defined at the junctions of the periodic elements. The number of these variables is related to the number of degrees of freedom (d.o.f.) which have been selected to represent the displacements, and also to the order of the differential equation of propagation, which in continuous media is equal to two. This set of variables can be looked upon as a "state vector" in relation to the spatial variable $z$. Generally, several equivalent choices are possible for this state vector. The state vector can, for instance, include pointwise displacements defined at the span junctions, their spatial derivatives, forces exchanged at these junctions, or various combinations of the above. In the case of track modelling,

following Pierre [17], we will choose as a state vector the coupled end displacements of the span:

$$\mathbf{U}_n = \begin{bmatrix} \mathbf{u}_{n-1} \\ \mathbf{u}_n \end{bmatrix}. \tag{1}$$

In equation (1) $\mathbf{u}_{n-1}$ and $\mathbf{u}_n$ denote, respectively, the displacement vectors of the end left and end right cross-sections of the $n$th rail span. At this point, the word "displacement" must be understood with a general meaning, and can include nodal displacements, global rotations or parameters of some displacement function.

Under the classical hypotheses of linearity and perfect periodicity, a matrix $\mathbf{T}$ can be defined so that the wave propagation equation takes the form

$$\mathbf{U}_{n+1} = \mathbf{T}\mathbf{U}_n. \tag{2}$$

This matrix is generally called the "transfer matrix" between consecutive spans. Clearly, its dimension is equal to the size of the state vector: i.e., twice the number of coupling co-ordinates defined at the junctions.

We will show at once how this transfer matrix can be built up for the railway track case. Here, the periodic structural element is composed of two consecutive half-sleepers, including their section of ballast and pads, and the embedded rail span (see Figure 2).

The end cross-sections of a rail span define its junctions with the adjacent spans, and some forces are exchanged between spans through these junctions. Let us denote by $f_n$ a vector representing the forces that the rail span $n+1$ exerts on the rail span $n$ through the junction $n$ (see Figure 3). Again, the word "force" must be understood with a general meaning, these forces being defined as the dual variables of the displacements introduced above.

Let us assume that the impedance matrix $\mathbf{Z}$ of the rail span, i.e., the matrix which relates the displacement vector of the span ends to the force vector applied on them, is known. This impedance matrix can be obtained in various ways through the use of analytical mechanics, finite element computations or other specific methods. Two examples of the development of such a transfer matrix will be presented in sections 3 and 4.

Thus, the inpedance equation of the rail span can be written:

$$\begin{bmatrix} -\mathbf{f}_{n-1} \\ \mathbf{f}_n \end{bmatrix} = \begin{bmatrix} \mathbf{Z}_{11} & \mathbf{Z}_{12} \\ \mathbf{Z}_{21} & \mathbf{Z}_{22} \end{bmatrix} \begin{bmatrix} \mathbf{u}_{n-1} \\ \mathbf{u}_n \end{bmatrix}, \tag{3}$$

with the classical symmetry property

$$\mathbf{Z}_{21} = \mathbf{Z}_{12}^{\mathrm{T}}.$$

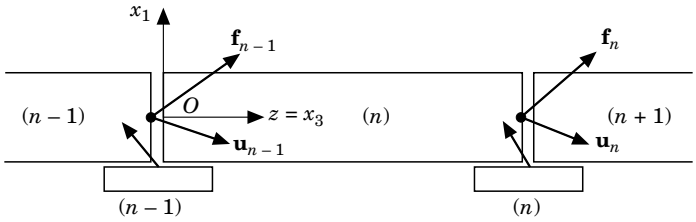


Figure 3. The force and dispacement vectors associated with coupling sections.

At a two-span junction, the force equilibrium equation must take into account the response of the support. We will assume that this response is symmetric with regard to the two adjacent spans, so that the periodic element is also symmetric. While not essential, this property—which is obviously fulfilled in the railway track case—entails interesting properties in vibration which will be briefly recalled in section 2.2

With account taken of the half-support impedances $\mathbf{H}/2$, the impedance equations applied to spans $n$ and $n+1$ result in

$$\begin{bmatrix} -\mathbf{f}_{n-1} \\ \mathbf{f}_n \end{bmatrix} = \mathbf{Z}^* \begin{bmatrix} \mathbf{u}_{n-1} \\ \mathbf{u}_n \end{bmatrix}, \qquad \begin{bmatrix} -\mathbf{f}_n \\ \mathbf{f}_{n+1} \end{bmatrix} = \mathbf{Z}^* \begin{bmatrix} \mathbf{u}_n \\ \mathbf{u}_{n+1} \end{bmatrix}, \tag{4}$$

with

$$\mathbf{Z}^* = \begin{bmatrix} \mathbf{Z}_{11} + \mathbf{H}/2 & \mathbf{Z}_{12} \\ \mathbf{Z}_{21} & \mathbf{Z}_{22} + \mathbf{H}/2 \end{bmatrix}. \tag{5}$$

The identification of the two expressions for $f_n$ in equations (4) and (5) leads to the recursive equation

$$\mathbf{Z}_{21}\mathbf{u}_{n-1} + (\mathbf{Z}_{11} + \mathbf{Z}_{22} + \mathbf{H})\mathbf{u}_n + \mathbf{Z}_{12}\mathbf{u}_{n+1} = 0. \tag{6}$$

From the definition of $\mathbf{T}$ in equation (2), the transfer matrix is found:

$$\mathbf{T} = \begin{bmatrix} \mathbf{0} & \mathbf{I} \\ -\mathbf{Z}_{12}^{-1}\mathbf{Z}_{21} & -\mathbf{Z}_{12}^{-1}(\mathbf{Z}_{11} + \mathbf{Z}_{22} + \mathbf{H}) \end{bmatrix}. \tag{7}$$

Therefore, knowing the impedance matrices of the support $\mathbf{H}$ and of the rail span $\mathbf{Z}$, we can completely determine the transfer matrix between adjacent spans.

### 2.2. CHARACTERISTIC WAVES

The eigenanalysis of the transfer matrix considerably clarifies the picture of free wave propagation, and leads to the definition of a set of uncoupled waves called "characteristic waves".

Let us consider a wave generated at the cross-section 0 travelling throughout the structure. Equation (2) results in

$$\mathbf{U}_n = \mathbf{T}^n \mathbf{U}_o. \tag{8}$$

With $\mathbf{\Lambda}$ defined as the diagonal matrix of the eigenvalues $\lambda_i$ and $\mathbf{\Phi}$ the square matrix of the eigenvectors $\mathbf{\Phi}_i$ of $\mathbf{T}$, this equation can be rewritten in the uncoupled form:

$$\mathbf{V}_n = \mathbf{\Lambda}^n \mathbf{V}_0, \tag{9}$$

with

$$\mathbf{V}_k = \mathbf{\Phi}^{-1}\mathbf{U}_k, \qquad \mathbf{\Lambda} = \mathbf{\Phi}^{-1}\mathbf{T}\mathbf{\Phi}. \tag{10}$$

A pair $(\lambda_i, \mathbf{\Phi}_i)$ defines a characteristic wave of the structure. The vector $\mathbf{\Phi}_i$ defines the shape of the characteristic wave $i$ over the cross-section, while the complex eigenvalue $\lambda_i$ defines the wavelength by its argument and the attenuation in the $z$-direction by its modulus. In a mechanical structure, it can be proved [10] that these eigenvalues appear in inverse pairs $(\lambda_i, 1/\lambda_i)$, corresponding respectively to left travelling and right travelling waves. In addition, if the matrix $\mathbf{T}$ is real—which depends on the damping hypotheses—the eigenvalues occur either in real values or in complex conjugate pairs.

The eigenvalue $\lambda_i$ is usually written in the exponential form $\lambda_i = \exp(\mu_i)$. For a wave travelling in the positive $z$-direction, the real part of the exponent $\mu_i$ must be negative, and has the meaning of an attenuation factor. On the other hand, the imaginary part has the meaning of a phase shift between two consecutive spans. As has been shown by several authors, a non-zero real part corresponds, on the frequency axis, to stop-bands, while a pure imaginary exponent corresponds to pass-bands. An interesting property was shown by Mead [15, 8] whereby, in case of a symmetric periodic element, the frontier frequencies belong to the set of resonance frequencies of the single element with specific boundary conditions. In a symmetric deformation of a span, a group of d.o.f.—lateral displacements, for instance—are symmetric: let us call these symmetric d.o.f. The others are—lateral rotations, for instance—antisymmetric: let us call these antisymetric d.o.f. The boundary conditions corresponding to the frontier frequencies are: (i) symmetric d.o.f. are locked while antisymmetric d.o.f. are free; (ii) antisymmetric d.o.f. are locked while symmetric d.o.f. are free. The first case corresponds generally to the well known pinned–pinned frequency. This property will become very useful for practical interpretations of the numerical results.

From this notion we can understand precisely how motion propagates along the track. Let us expand the state vector of the $n$th span on the basis of the eigenvectors $\mathbf{\Phi}_i$:

$$\mathbf{U}_n = \begin{bmatrix} \mathbf{u}_{n-1} \\ \mathbf{u}_n \end{bmatrix} = \mathbf{\Phi V}. \tag{11}$$

From the property of eigenvectors, we have also

$$\mathbf{U}_{n+1} = \begin{bmatrix} \mathbf{u}_n \\ \mathbf{u}_{n+1} \end{bmatrix} = \mathbf{\Phi \Lambda V}. \tag{12}$$

Now let us split the matrices $\mathbf{\Phi}$, $\mathbf{\Lambda}$ and the vector $\mathbf{V}$ as follows:

$$\mathbf{\Phi} = \begin{bmatrix} \boldsymbol{\varphi}'^R & \boldsymbol{\varphi}'^L \\ \boldsymbol{\varphi}^R & \boldsymbol{\varphi}^L \end{bmatrix}, \qquad \mathbf{\Lambda} = \begin{bmatrix} \boldsymbol{\lambda} & \\ & \boldsymbol{\lambda}^{-1} \end{bmatrix}, \quad \mathbf{V} = \begin{bmatrix} \boldsymbol{\alpha} \\ \boldsymbol{\beta} \end{bmatrix}, \tag{13}$$

where the superscripts $R$ and $L$ denote the right and left eigenvectors, associated respectively with the right and left travelling waves. The submatrix $\boldsymbol{\lambda}$ is a diagonal matrix including only the modulus eigenvalues less than one (right travelling waves).

From equations (11) and (12) we can write

$$\mathbf{u}_n = \alpha_i \boldsymbol{\varphi}_i^R + \beta_i \boldsymbol{\varphi}_i^L, \qquad \mathbf{u}_{n+1} = \lambda_i \alpha_i \boldsymbol{\varphi}_i^R + (1/\lambda_i)\beta_i \boldsymbol{\varphi}_i^L, \tag{14a, b}$$

where implicit summation with respect to index $i$ is assumed. Equation (14a) expresses the displacements of the junction $n$ as a combination of right and left travelling waves. Equation (14b) shows how the right travelling waves decrease, while the left travelling waves increase in the positive $z$-direction.

These equations can be directly rewritten in terms of forces. By using equations (4) while taking into account equations (14), it is easy to find that

$$\mathbf{f}_n = \alpha_i \mathbf{g}_i^R + \beta_i \mathbf{g}_i^L, \qquad \mathbf{f}_{n+1} = \lambda_i \alpha_i \mathbf{g}_i^R + (1/\lambda_i)\beta_i \mathbf{g}_i^L, \tag{15a, b}$$

where the following notation has been used:

$$\mathbf{g}_i^R = -\left(\mathbf{Z}_{11} + \frac{\mathbf{H}}{2} + \lambda_i \mathbf{Z}_{12}\right)\boldsymbol{\varphi}_i^R = \left(\frac{1}{\lambda_i}\mathbf{Z}_{21} + \mathbf{Z}_{22} + \frac{\mathbf{H}}{2}\right)\boldsymbol{\varphi}_i^R, \tag{16a}$$

$$\mathbf{g}_i^L = -\left(\mathbf{Z}_{11} + \frac{\mathbf{H}}{2} + \frac{1}{\lambda_i}\mathbf{Z}_{12}\right)\boldsymbol{\varphi}_i^L = \left(\lambda_i \mathbf{Z}_{21} + \mathbf{Z}_{22} + \frac{\mathbf{H}}{2}\right)\boldsymbol{\varphi}_i^L, \tag{16b}$$

The equations (16) must be understood to be without summation on the index $i$.

### 2.3. RECEPTANCE COMPUTATION

In experimental terms, an excitation $F(t)$—generally a hammer strike—is applied at some point $P$, the measured response $u(t)$ being the displacement of another point $Q$ on the rail. It is thus necessary to know the transfer function—the receptance—between $P$ and $Q$. This function can be easily determined from the dynamic equilibrium of the beam length comprised betwen these points. In the case in which $P$ and $Q$ belong to the same cross-section, this beam length is reduced to an infinitesimal slice of rail around the point. This procedure leads to a relation $\mathbf{u} = \mathbf{H}_{PQ}(\omega)\mathbf{F}$. The derivation of the function $\mathbf{H}_{PQ}(\omega)$ is detailed in Appendix A, in the case in which $P$ and $Q$ are identical. The reader can easily extend the method to the cases in which $P$ and $Q$ are distinct.

## 3. MODEL BASED ON THE CLASSICAL BEAM THEORY

In this section the previous formulation will be applied to a real case. The transfer matrix will be built according to the classical Euler–Bernouilli and Timoshenko models, and for validation, the data set will be taken from the literature. For an experimental validation, another data set will be used, for which experimental measures are available.

### 3.1. TRANSFER MATRIX OF THE RAILWAY TRACK

As was shown above, the transfer matrix of the track span is built from the impedance matrices of the rail span and supports. Here, the impedance matrix of the rail span is developed analytically by using a classical method [18]. Two models are generally used.

(1) *Euler–Bernouilli beam*. In this model one assumes that the cross-sections remain plane and orthogonal to the beam mean line. Shearing effects are neglected in this model.

(2) *Timoshenko beam*. This model takes into account the shearing effects through a modification of the strain energy expression. This modification leads to the notion of reduced section and the classical coefficients associated with it.

The torsion phenomenon can be incorporated into these models through the introduction of a torsion modulus $J$.

Let us remark that, in these models, the degrees of freedom (d.o.f.) of the rail cross-section are the two transverse displacements and the three rotations of the section.

Concerning the lateral vibration, a problem arises. How can the classical coupling effects between shearing and torsional effects be accounted for in relation with the location of the shear center? Because the classical beam models do not have a pure kinematic origin, these effects cannot be easily integrated within a consistent theory. For the time being, these coupling effects will be ignored, but this important question will be the key point of section 4.

The development of the impedance matrix, starting from the equations of motion, is standard. The method is recalled in Appendix B.

From the impedance matrix, a transfer matrix of size $10 \times 10$ can be assembled as in equation (7).

### 3.2. EIGENANALYSIS OF THE TRANSFER MATRIX

When we applied the theory to real data, we immediately encountered a numerical problem, related to the very nature of the mathematical equations.

The transfer matrix $\mathbf{T}$ defined in equation (7) is non-symmetric. The computation of its eigenvalues and eigenvectors can be performed by using some classical algorithms of eigenanalysis. However, due to the existence of inverse eigenvalues, the matrix $\mathbf{T}$ is liable to be ill-conditioned, even in ordinary situations. For instance let us assume that the (dimensionless) lowest eigenvalue lies in the $10^{-8}$ range, which happens currently for a near-field wave and is probably of little physical interest. Then a $10^{8}$ range eigenvalue necessarily exists, corresponding to the wave in the opposite direction. Therefore the eigenvalue spectrum covers a 16-digit range, which entails an ill-conditioned matrix, and therefore ill-determined eigenvectors.

In the case of a railway track, using the simplest rail model with the current mechanical characteristics of rail and supports, the eigenvalue spectrum was found to cover a 14-digit range. When working on a 64-bit computer, numerical problems were encountered beyond a frequency of 2300 Hz.

Various methods can be used to cope with this problem. The most natural one would be to take advantage of the structure of the characteristic polynomial. Because of the existence of pairs of inverse roots, the degree $2n$ characteristic polynomial can be reduced to a degree $n$ polynomial of the unknowns $s_i = \lambda_i + 1/\lambda_i$. The roots of this polynomial provide the eigenvalues through a simple second degree equation, and then the matrix of eigenvectors through a linear system. The drawback of the method is that it does not allow the use of classical eigenanalysis packages. Therefore another method was developed by forming the auxiliary matrix $\mathbf{T}^* = \mathbf{T} + \mathbf{T}^{-1}$, the eigenvalues $\lambda_i^*$ of which are related to two inverse eigenvalues $\lambda_i$ of $\mathbf{T}$ according to $\lambda_i^* = \lambda_i + \lambda_{n+i} = \lambda_i + 1/\lambda_i$, and so occur in pairs of equal values.

It can be objected that the supposedly ill-conditioned matrix $\mathbf{T}$ will prevent its inverse $\mathbf{T}^{-1}$ from being computed correctly. Actually, for the matrix $\mathbf{T}$ defined by equation (3), its inverse matrix can be formally expressed as

$$\mathbf{T}^{-1} = \begin{bmatrix} -(\mathbf{Z}_{11} + \mathbf{Z}_{22} + \mathbf{H})^{-1}\mathbf{Z}_{21} & -(\mathbf{Z}_{11} + \mathbf{Z}_{22} + \mathbf{H})^{-1}\mathbf{Z}_{12} \\ \mathbf{I} & \mathbf{0} \end{bmatrix},$$

As the submatrices $\mathbf{Z}_{11}$, $\mathbf{Z}_{22}$ and $\mathbf{H}$ are not usually ill-conditioned, the inversion can be accurately performed.

The eigenvectors of $\mathbf{T}$ correspond in pairs $\mathbf{\Psi}_i = (\mathbf{\Phi}_i, \mathbf{\Phi}_{n+i})$ with the eigenvectors of $\mathbf{T}^*$ to form $n$ eigenspaces of dimension 2 associated with the $n$ double eigenvalues $\lambda_i^*$. Of course, a standard eigenanalysis computer code provides two arbitrary independent combinations $\mathbf{\Phi}_i'$ and $\mathbf{\Phi}_i''$ of $\mathbf{\Phi}_i$ and $\mathbf{\Phi}_{n+i}$, associated with the double eigenvalue $\lambda_i^*$, so that a problem occurs when restoring the original pairs $\mathbf{\Psi}_i$.

Upon expanding the eigenvector $\mathbf{\Phi}_i$ on the basis $\mathbf{\Phi}_i'$, $\mathbf{\Phi}_i''$, as $\mathbf{\Phi}_i = \xi\mathbf{\Phi}_i' + \eta\mathbf{\Phi}_i''$, the problem results in the determination of the complex components $\xi$ and $\eta$. With $\mathbf{\Phi}_i$ written as eigenvector of $\mathbf{T}$,

$$\xi(\mathbf{T} - \lambda_i\mathbf{I})\mathbf{\Phi}_i' + \eta(\mathbf{T} - \lambda_i\mathbf{I})\mathbf{\Phi}_i'' = \mathbf{0}, \tag{17}$$

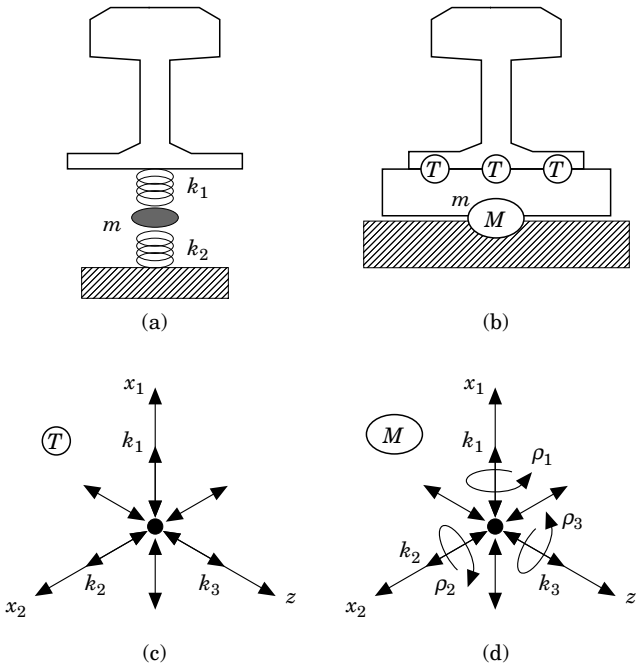


Figure 4. The support models for computation: (a) model with two simple springs and one mass; (b) model with four multi-directional springs of types ($T$) and ($M$); (c) the principle of the three-directional spring of type ($T$); (d) principle of the mixed longitudinal–rotating spring of type ($M$).

$\xi$ and $\eta$ can be determined proportionally from a single line of equation (17). Actually, because of the frequent occurrence of near-zero lines, they are better determined after making the dot product of equation (17) by $\mathbf{\Phi}_i'$ or $\mathbf{\Phi}_i''$.

In practice, the modulus eigenvalues less than one can be considered first, their corresponding eigenvectors being determined by the previous method. They represent waves travelling in the positive $z$-direction—let us say, right travelling waves—the left travelling waves being associated with the inverse eigenvalues. The corresponding eigenvectors, in the case of symmetric periodic elements, can be deduced from the right travelling waves by using simple rules of symmetry. In the terminology of section 2.2, the symmetric d.o.f. $u_1$, $u_2$ and $\theta_3$ are taken with the same sign, and the antisymmetric d.o.f. $u_3$, $\theta_1$ and $\theta_2$ are taken with the opposite signs.

### 3.3. COMPUTATIONAL RESULTS

From the above theory, a first sequence of computations was performed to validate the method by comparison with some results from the literature and with experimental measurements delivered by the industrial partner.

The first data set used was identical to that given by Heckl [19]. The rail characteristics are the following: section $7{\cdot}484 \times 10^{-3}$, vertical and lateral inertia $49{\cdot}932 \times 10^{-3}$ and $2{\cdot}971 \times 10^{-3}$, and vertical and lateral Timoshenko modulus 0·6 and 0·8. The support reduces to a simple spring–mass–spring system (see Figure 4(a)) with the following characteristics: mass 162 kg, spring stiffnesses (N/m) $3{\cdot}8 \times 10^8$ and $0{\cdot}75 \times 10^8$. The computational option is the Timoshenko model.

Let us first consider the characteristic waves. Due to the nature of the Timoshenko model, vertical, lateral and torsional waves are uncoupled in the analysis. The spectra of the attenuation factors which are found for the two vertical waves are shown in Figure 5.

These results can be compared with the similar curves presented in reference [19]. As expected, results are strictly identical. If we now consider the receptance spectrum of the track for a vertical excitation applied on the top of the rail in front of a support (not drawn), once more it is found that the computed spectrum exactly matches the curve given in reference [19].

At this point, the present model and the Heckl model [19] are strictly identical. In fact, they differ only in their algebraic organization. However, the advantages of the transfer matrix method are clear. They were largely outlined by Pierre *et al*. [11, 17]. The impedance matrix of the periodic element is developed independently, and so can take into account any sophisticated features of the mechanical model. For example, the extended model developed in section 4 will naturally take its place in the model. Moreover, as has been shown by several authors, the transfer matrix method can easily be adapted to closely related problems; for instance, in the case of a finite number of elements, or in the case of slightly varying elements.

To compare with experimental results, another data set is introduced, for which an experimental analysis is available. The rail characteristics are unchanged, but the transfer matrix of the support is enriched (see Figures 4(b)–(d)). Sleepers and pads are represented by a set of three springs ($T$), each one having three-directional longitudinal effects (see Figures 4(b), (c) and (d)). The distance of the exterior springs to the symmetry axis is 4·37 cm. The stiffness and damping coefficients of these springs in the lateral, vertical and axial directions are ($2{\cdot}0 \times 10^9$, 0·1), ($4{\cdot}5 \times 10^8$, 0·8) and ($7{\cdot}5 \times 10^8$, 0·1). The ballast is represented by a central spring ($M$) having three-directional longitudinal and rotational effects. The stiffness and damping coefficients of this spring in the lateral, vertical and axial directions are, in translation, ($7{\cdot}5 \times 10^7$, 0·4), ($8{\cdot}5 \times 10^8$, 0·4) and ($7{\cdot}5 \times 10^7$, 0·1) and, in rotation, ($8{\cdot}0 \times 10^8$, 0·4), ($8{\cdot}5 \times 10^8$, 0·4) and ($9{\cdot}5 \times 10^7$, 0·1). The mass and the three principal inertia of the ballast are 122, 0·635, 1·322 and 1·144 respectively (S.I. Units).

Let us assume a vertical excitation applied at the top of the cross-section in front of a support. In Figure 11(b) (of section 4, as are Figures 12–14) is shown the computed accelerance spectrum, while in Figure 12(b) is shown the experimental one in the same case. Globally, these results present a satisfactory agreement, especially in the low half-frequency range. However, a detailed examination shows that the computed spectrum

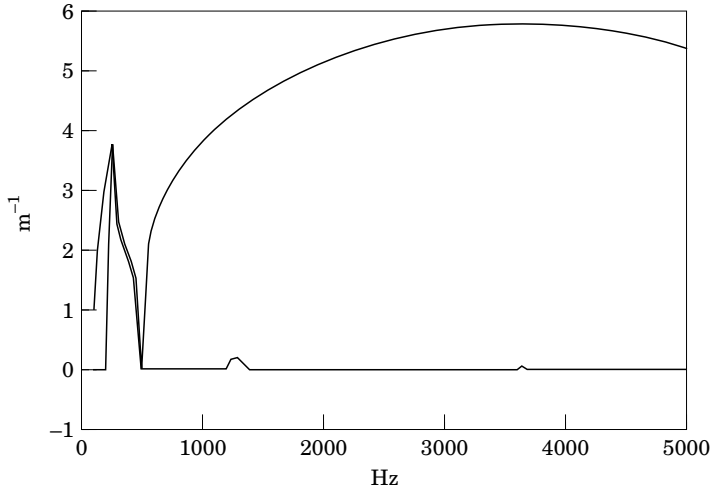


Figure 5. The attenuation factors of the two vertical characteristic waves: the case of a Timoshenko model.

cuts off some high frequency peaks–beyond 1200 Hz—that exist in the experimental one. This is a first element to suggest some insufficiency of the model.

Now the excitation is applied at the same point in the lateral direction. The computed spectrum for a Timoshenko beam is shown in Figure 13(a), while the experimental results are presented in Figure 14(a). Here, the two spectra present a global 10 dB difference on the accelerance axis. Of course, the first idea is to attribute the gap to our insufficient knowledge of the support characteristics. Actually, a large computational investigation showed that no combination of these parameters could substantially improve the result.

On the other hand, simple modifications of the energy expression were tried in order to incorporate the coupling effects attached to the location of the shear center. To summarize, it was found that the incorporation of such effects could sufficiently raise the global level of the accelerance spectrum. Unfortunately, these manipulations could not be formalized within the frame of a consistent theory. A non-symmetric impedance matrix was generally encountered, and finally poorly accurate results were found.

At this point, it became obvious that the poor kinematics involved in the model was the main cause of the trouble, so that a reconsideration of the theory was necessary. In the classical beam models, the kinematics of the beam is essentially restricted to the set of rigid body motions of the cross-sections. Although the Timoshenko model does not have a pure kinematic assessment, it can be interpreted as an improvement of a kinematic model with six d.o.f.—three translational and three rotational—through the introduction of appropriate shearing factors. On the other hand, not all modes involving cross-section deformation—warping effects, for instance—can be directly incorporated into these models, which generally results in structural inconsistencies and in excessive stiffness of the model.

For these reasons, a new approach based on an enriched kinematic model was deemed necessary. We will see that its application resulted immediately in a substantial improvement of the results. The next part of this paper is devoted to this extension.

## 4. MODEL BASED ON A KINEMATIC FORMULATION

In this section, the equations of the beam deformation will be reformulated on a pure kinematic basis. The advantage of this approach is that the basic set of rigid body modes of the cross-section can be enriched by addition of suitable deformation modes. In this framework, the elastodynamics of the rail will be redeveloped so as to provide the new transfer matrix needed by the periodic analysis. Finally, the quality of the model will be discussed from comparison with experimental results.

### 4.1. NOTION OF ''CROSS-SECTION MODE''

A refined track representation necessarily involves some finite element discretization of the rail. We have already recalled the drawbacks of the method which was followed by Thompson [3], starting from a complete discretization of the rail span. In contrast, the method developed below needs only discretization of the cross-section.

The basic idea of this new method lies in the intuitive notion of ''cross-section mode''. Basically, it is assumed that, disregarding local effects, the rail's cross-section possesses some preferential shapes of deformation. In other words, these modes define a reduced basis for the space of displacements of the cross-section. Obviously, the quality of the subsequent analysis depends heavily on an optimal choice of this reduced basis.

How to obtain these modes is a question that can receive simple answers as well as sophisticated answers. For instance, the usual theory of beams suggests a set of rigid body modes which must necessarily belong to the reduced basis: translations and rotations of

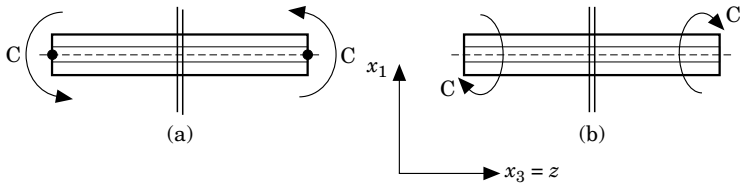


Figure 6. The static computational cases used to provide extra modes: (a) shearing mode; (b) torsional mode.

the $x_1$ and $x_2$ directions must at least be selected to represent the classical bending modes. Longitudinal $z$-translation must be introduced to represent the longitudinal mode. Conversely, these rigid body modes are sufficient to provide a satisfactory representation of the coresponding effects.

On the other hand, it is well known that shearing and torsional patterns cannot be well represented by the pure rigid body kinematics of the cross section, since warping is an essential feature of these phenomena. Moreover, classical beam theory shows that these two effects have a mutual interaction, leading to the notion of shear center. Due to the non-symmetric nature of the rail profile under lateral loading, these aspects must be highly relevant to the present case.

In the present paper, in addition to the development of a general methodology, the purpose will be restricted to a correct treatment of the basic phenomena of low frequency beam mechanics—pure extensional, bending, shearing and torsional deformations. To ensure a correct treatment of the shearing and torsional effects, suitable additional modes must be selected to enrich the kinematics. In the low frequency range, it can be expected that these additional modes will not be very different from what they are in pure static deformation. This leads us simply to extract the needed additional modes from a set of static computations, by using a standard F.E. code.

The static F.E. computation which was performed to provide the shearing mode is shown in Figure 6(a). A simply supported 60 cm rail length is submitted to equal end bending moments. The shearing pattern is extracted from the displacement vector of the mid-length cross-section. Actually, it is found that the mode can be reduced numerically to its $z$-components (S mode).

The static F.E. computation which was performed to provide the torsional mode is shown in Figure 6(b). Again, a 60 cm rail length is submitted to opposite longitudinal moments. The torsional pattern is still extracted at the mid-length cross-section and, consistently with the classical torsion theory, can be reduced to the $z$-displacements (warping).

Obviously, the high frequency range will not be covered with the present reduced basis, since for high frequencies the appropriate additional modes cannot be determined from static computations. Therefore in the high frequency range a different method is needed to complete the reduced basis. Several methods can be used to reach this target. Probably the most powerful method would be to perform a separate analysis of the free rail vibration, and then select a set of significant modes to form a suitable reduced basis. At the present time, this approach is under development, and definite results are not available. This paper will thus be restricted to a low frequency analysis. As we shall see below, the present method was sufficient to provide satisfying results in the 0–1200 Hz range.

To summarize, we will assume that the displacement field is defined by a system of the form

$$u = a_m(z, t)u^m(x_1, x_2), \tag{18}$$

where implicit summation with respect to the index $m$ is assumed (see Figure 7). The functions $u^m(x_1, x_2)$, which are defined on the rail cross-section, represent the chosen cross-section modes. When extracted from a F.E. analysis, they are defined for each element by interpolation from nodal values.

A question arises as to whether this representation is mechanically acceptable; for instance, if the condition of a free outer surface is automatically fulfilled. Actually, the structure has, in the cross-section plane, no more degrees of freedom than the size of the reduced basis, which is very small. In general, it is thus theoretically impossible precisely to fulfil the surface condition in such a reduced space. Nor is it possible to fulfil in detail all of the conditions for internal equilibrium. This explains the choice which was made above of selecting static deformation modes, which by themselves are consistent solutions of physical problems. The approximation introduced here is the same as in the classical beam theory: disregarding local effects, it is assumed that the beam deformation can be obtained, with good accuracy, from the solutions of tractional, bending, shearing and torsional problems—solutions which depend only on the shape of the cross-section. It is equivalent to assume that this reduced basis is sufficient to ensure, although approximately, the physical consistency of the solution, including the free outer surface conditions, as well as the internal equilibrium conditions.

To summarize, the modes $u^m(x_1, x_2)$ must be drawn from consistent and representative mechanical problems so as to be acceptable modes.

### 4.2. FREE RAIL DYNAMICS

It was shown in section 2 that an important step towards a periodic model analysis is the determination of the transfer matrix, which is derived directly from the determination of the rail span impedance matrix. Because of the non-classical kinematic model (18), the determination of this impedance matrix requires a complete reformulation of the elastodynamics of the rail.

Equation (18) defines a displacement function by its co-ordinates $a_m(z, t)$ on the set of basic functions. Note that, similarly, a field of forces $f(x_1, x_2, z, t)$ can be characterized by

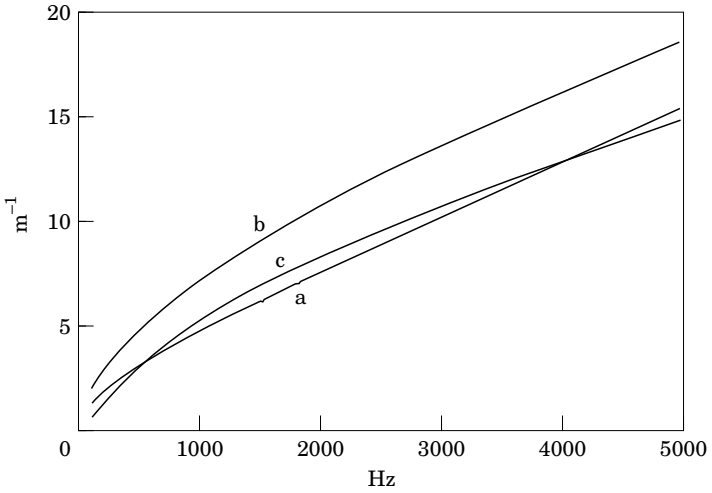


Figure 7. The wavenumbers of the propagating waves of the free infinite rail; (a) vertical bending mode; (b) lateral bending mode; (c) torsional mode.

a set of dual co-ordinates $b_m(z, t)$. Let us introduce the virtual work per unit length of the beam $\delta W(z, t)$:

$$\delta W(z, t) = \iint_s f(x_1, x_2, z, t)\, \delta u(x_1, x_2, z) \mathrm{d}S.$$

The force co-ordinates $b_m(z, t)$ follow from equation (18):

$$\delta W(z, t) = \delta a_m(z, t) \iint_s f(x_1, x_2, z, t) u^m(x_1, x_2) \mathrm{d}S = \delta a_m(z, t) b_m(z, t). \tag{19}$$

The development of elastodynamics is classical in continuum mechanics. The specificity is that the longitudinal co-ordinate $z$ must be separated from the others in the equations. Upon assuming a virtual displacement defined by the function $\delta u = \delta a_m(z) u^m(x_1, x_2)$, and denoting by $\sigma_{pq}$ and $\varepsilon_{pq}$ the stress and strain tensors in the body, the associated virtual work can be computed from

$$\delta W = \iiint_v \sigma_{ij} \delta \varepsilon_{ij} \, \mathrm{d}V, \tag{20}$$

where $V$ denotes the volume of the body.

In the following development, it will be more convenient to refer to the $z$ co-ordinate with an indexed variable, by assuming $z = x_3$ (see Figure 3).

The strain expressions can be written as

$$\begin{aligned}
&\varepsilon_{ij} = \tfrac{1}{2} a_m (u^m_{i,j} + u^m_{j,i}), \qquad i, j = 1, 2,\\
&\varepsilon_{i3} = \varepsilon_{3i} = \tfrac{1}{2} (a_m u^m_{3,i} + a'_m u^m_i), \qquad i = 1, 2,\\
&\varepsilon_{33} = a'_m u^m_3,
\end{aligned} \tag{21}$$

where the notation $f_{,i}$ denotes the derivative of the function $f$ with respect to the $x_i$ co-ordinate, and $a'$ the derivative of the function $a(z, t)$ with respect to $z$.

The stress tensor is obtained from the Lamé equation $\sigma_{ij} = \lambda \theta \delta_{ij} + 2\mu \varepsilon_{ij}$, where $\lambda$ and $\mu$ are the Lamé coefficients, $\delta_{ij}$ is the Kronecker symbol and $\theta$ is the first invariant of the strain tensor. From equation (21) we find that

$$\begin{aligned}
&\sigma_{ij} = [\lambda \delta_{ij} u^m_{p,p} + \mu (u^m_{i,j} + u^m_{j,i})] a_m + \lambda \delta_{ij} u^m_3 a'_m, \qquad i, j = 1, 2,\\
&\sigma_{i3} = \sigma_{3i} = \mu u^m_{3,i} a_m + \mu u^m_i a'_m, \qquad i = 1, 2,\\
&\sigma_{33} = \lambda u^m_{p,p} a_m + (\lambda + 2\mu) u^m_e a'_m.
\end{aligned} \tag{22}$$

Let us form the equilibrium equation for a finite length $(0, L)$ of the beam. Upon using equations (21) and (22) in equation (20), the virtual work of internal forces can be written as

$$\delta W_{int} = \delta W_1 + \delta W_2 + \delta W_3 + \delta W_4, \tag{23}$$

with

$$\delta W_1 = A_{mn}\int_0^L a_m(z,\,t)\delta a_n(z)\mathrm{d}z, \qquad \delta W_2 = B_{mn}\int_0^L a'_m(z,\,t)\delta a_n(z)\mathrm{d}z,$$

$$\delta W_3 = C_{mn}\int_0^L a_m(z,\,t)\delta a'_n(z)\mathrm{d}z, \qquad \delta W_4 = D_{mn}\int_0^L a'_m(z,\,t)\delta a'_n(z)\mathrm{d}z, \tag{24}$$

where the coefficients $A_{mn}$, $B_{mn}$, $C_{mn}$ and $D_{mn}$ are expressed, from equations (21) and (22), as

$$A_{mn} = \tfrac{1}{2}\iint_s \{[\lambda\delta_{ij}u^m_{p,p} + \mu(u^m_{i,j} + u^m_{j,i})][u^n_{i,j} + u^n_{j,i}] + \mu u^m_{3,i}u^n_{3,i}\}\,\mathrm{d}S,$$

$$B_{mn} = C_{nm} = \tfrac{1}{2}\iint_s \{\lambda\delta_{ij}u^m_3(u^n_{i,j} + u^n_{j,i}) + \mu u^m_1 u^n_{3,i}\}\,\mathrm{d}S,$$

$$D_{mn} = \tfrac{1}{2}\iint_s \{\mu u^m_{3,i}u^n_1 + 2\lambda u^m_{p,p}u^n_{3,i}\}\,\mathrm{d}S. \tag{25}$$

Integrating the two last terms in equation (23) by parts leads to

$$\delta W_{int} = \int_0^L [A_{mn}a_m(z,\,t) + (B_{mn} - C_{mn})a'_m(z,\,t) - D_{mn}a''_{mn}(z,\,t)]\delta a_n(z)\mathrm{d}z - V^n_0(t)\delta a_n(0) + V^n_L(t)\delta a_n(L), \tag{26}$$

with

$$V^n_0(t) = C_{mn}a_m(0,\,t) + D_{mn}a'_m(0,\,t), \qquad V^n_L(t) = C_{mn}a_m(L,\,t) + D_{mn}a'_m(L,\,t). \tag{27}$$

Hence the dynamic equation splits into the following relations:

$$A_{mn}a_m(z,\,t) + (B_{mn} - C_{mn})a'_m(z,\,t) - D_{mn}a''_m(z,\,t) = b_n(z,\,t), \tag{28}$$

$$V^n_0(t) = -b_n(0,\,t), \qquad V^n_L(t) = b_n(L,\,t). \tag{29}$$

At the span ends (see Figure 3), the generalized force vector $\mathbf{b}(b_1, b_2, \ldots, b_N)$ represents the forces associated with end faces. Dropping the indexes so as to form the corresponding vectors and matrices, we can write

$$-f_0(t) = b(0,\,t) = V_0(t) = Ca(0,\,t) + Da'(0,\,t),$$
$$f_L(t) = b(L,\,t) = V_L(t) = Ca(L,\,t) + Da'(L,\,t). \tag{30}$$

If the rail length is free of external forces (free wave propagation equation), the right side of equation (28) includes inertial forces only:

$$b_n(z,\,t) = M_{mn}a_m(z,\,t), \tag{31}$$

with

$$M_{mn} = \rho \iint_s u^m(x_1, x_2)u^n(x_1, x_2)\mathrm{d}S. \tag{32}$$

Taking the Fourier transforms with respect to $z$, and then the Fourier transforms with respect to $t$ of the two sides of equation (28), yields the free wave propagation equation in the form

$$[\mathbf{A} - \omega^2\mathbf{M} + \mathrm{j}k(\mathbf{B} - \mathbf{C}) - k^2\mathbf{D}]\mathbf{a} = \mathbf{0}, \tag{33}$$

where **A**, **B**, **C**, **D** and **M** denote the matrices defined in equations (25) and (32), **a** the vector of Fourier transforms $a_m$ of displacement co-ordinates and $k$ a complex factor characterizing the wavelength and attenuation.

This equation defines a classical problem of eigenvalues and eigenvectors. Because of the skew-symmetric nature of the matrix $\mathbf{B} - \mathbf{C}$, it is easy to show that, if **a** has dimension $n$, the $2n$ eigenvalues occur in opposite pairs.

With equation (33) written in the form

$$\begin{bmatrix} \mathbf{0} & \mathbf{I} \\ \mathbf{D}^{-1}(\omega^2\mathbf{M} - \mathbf{A}) & \mathbf{D}^{-1}(\mathbf{C} - \mathbf{B}) \end{bmatrix} \begin{bmatrix} \mathbf{a} \\ \mathrm{j}k\mathbf{a} \end{bmatrix} = \mathrm{j}k \begin{bmatrix} \mathbf{a} \\ \mathrm{j}k\mathbf{a} \end{bmatrix}, \tag{34}$$

$k$ and **a** are found from eigenanalysis of the left side real matrix. Let $k_i$ be a complex value and let $\mathbf{a}_i^*$ be the associated vector derived from equation (34); any solution wave can be defined by its co-ordinates $\alpha_p$:

$$a(z) = \alpha_p a^{*p}\, \mathrm{e}^{\mathrm{j}k_p z}, \tag{35}$$

where $a(z)$ denotes the Fourier transform with respect to time of the function $a(z, t)$. This notation will be used systematically below, along with any time dependent function $g(x, y, \ldots, t)$: its Fourier transform is denoted by $g(x, y, \ldots)$, by simply dropping the $t$ variable.

### 4.3. TRANSFER MATRIX OF THE RAIL SPAN

Now the construction of the span impedance matrix follows the consideration of end conditions. From equation (35), the end displacement co-ordinates are defined on the eigenvector basis by

$$\begin{aligned} a(0) &= \alpha_p a^{*p}, \qquad a(L) = \alpha_p\, \mathrm{e}^{\mathrm{j}k_p L} a^{*p}, \\ a'(0) &= \alpha_p k_p a^{*p}, \qquad a'(L) = \alpha_p k_p\, \mathrm{e}^{\mathrm{j}k_p L} a^{*p}. \end{aligned} \tag{36}$$

The first two equations form a $2n$ order system which can be solved in $\alpha_p$. The result is then carried into the last two equations to give the relation

$$\begin{bmatrix} \mathbf{a}'(0) \\ \mathbf{a}'(L) \end{bmatrix} = \mathbf{G} \begin{bmatrix} \mathbf{a}(0) \\ \mathbf{a}(L) \end{bmatrix}.$$

Then, from equation (30), the impedance matrix $\mathbf{Z}$ is found:

$$\begin{bmatrix} -\mathbf{f}_0 \\ \mathbf{f}_L \end{bmatrix} = \mathbf{Z} \begin{bmatrix} \mathbf{a}(0) \\ \mathbf{a}(L) \end{bmatrix}. \tag{37}$$

This impedance matrix will be used to form the transfer matrix (7), and the receptance function defined in section 2.3. These calculations follow exactly the same development as in section 2.

### 4.4. IMPEDANCE MATRIX OF THE SUPPORTS

To build the transfer matrix of the track span, the impedance matrix of the support is needed. This transfer matrix must also be expressed in terms of the generalized displacements of the corresponding rail junction and their associated forces. All supports being assumed identical, the support 0 can be considered. Let us assume that its impedance matrix has been determined independently by means of experiments, spring–mass models, or both, and reduced to an expression on its median line $\Sigma$: $\mathbf{f} = \mathbf{Hu}$. From equation (18), the virtual work of $\mathbf{f}$ in a virtual displacement of the frontier has the form:

$$\mathbf{f} \cdot \delta\mathbf{u} = \left[ \int_\Sigma [\mathbf{H}\mathbf{u}_m(P_\Sigma)] \cdot \mathbf{u}_n(P_\Sigma) \mathrm{d}\Sigma \right] \mathbf{a}_m(0, t) \delta\mathbf{a}_n(0).$$

This expression defines the generalized co-ordinates of the response. Hence the support impedance is defined by the matrix

$$H_{mn} = \int_\Sigma [\mathbf{H}\mathbf{u}_m(P_\Sigma)] \cdot \mathbf{u}_n(P_\Sigma) \mathrm{d}\Sigma, \tag{38}$$

which can be readily carried into the span impedance matrix (5).

### 4.5. NUMERICAL APPLICATION: FREE WAVE ANALYSIS

The above method is now applied to the railway track case. The mechanical characteristics are given by the second data set of section 3.3. First, we will examine some aspects of the propagating free waves.

In the above model, free waves were encountered at two levels. A set of free waves and wavenumbers was determined in section 4.2, following the elastodynamic formulation. They represented the characteristic waves of the infinite rail without supports. Then, a set of characteristic waves was determined for the periodic structure including supports, providing the characteristic modes of the track and their attenuation factors.

Let us first examine the free waves of the infinite rail without supports. They are determined from equation (34) by using a model including rigid body modes—translations $u_1$ and $u_2$ and the three rotations—and the two additional modes defined in section 4.1: the vertical shearing mode and the torsional warping mode. The matrix equation is thus of size 14 and provides seven pairs of solutions with opposite wavenumbers, representing right and left travelling waves. A set of three waves in the vertical plane $x_1z$ (symmetry plane), which will be labelled "vertical waves", is found to be naturally uncoupled from the others. This set involves the $u_1$ translation, the $\theta_2$ rotation and the vertical shearing mode. The other four waves, which will be labelled "lateral waves", involve the $u_2$ translation, the $\theta_1$ and $\theta_3$ rotations and the warping mode of torsion.

It turns out that, of these seven waves, four have pure real wavenumbers—they correspond to nearfield waves. Three waves have pure imaginary wavenumbers—they represent propagating waves. The three wavenumber plots of the propagating waves are given in Figure 7, showing classical ascending curves. The numerical values have roughly

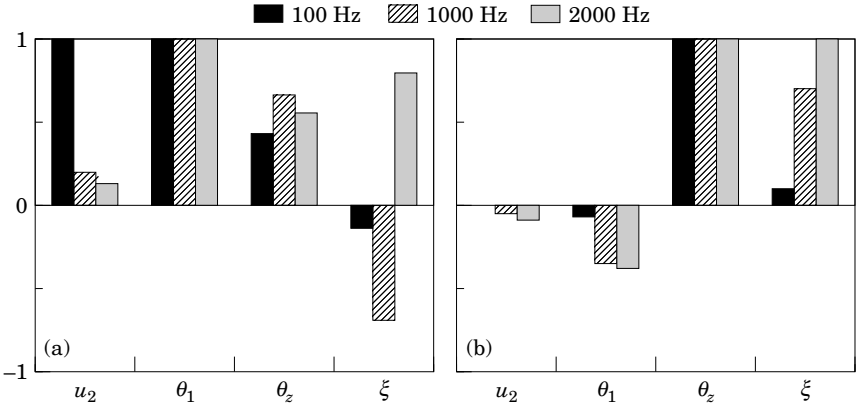


Figure 8. The relative compositions of the lateral propagating waves of the free infinite rail: (a) lateral bending mode; (b) torsional mode.

the same magnitudes as those given by Thompson, although the latter takes into account a two-layer continuous support. From inspection of the corresponding eigenvectors, the curves can easily be labelled "vertical, lateral bending waves", and "torsional wave". However, it must be observed that in the lateral direction the two propagating waves appear in fact to be variable "mixtures" of the different basic modes. To make a valid comparison of these "mixtures", there is an obvious problem of normalization. The various mode components, for example a lateral displacement and a warping mode coefficient, can hardly be compared through their numerical values. An "heuristic" normalization of the modes was performed by referring them to the highest value that they reached throughout the results. The wave compositions obtained are shown in Figure 8 for three frequency values of 100, 1000 and 2000 Hz. It can be seen that bending and torsional effects remain always coupled together, although in variable proportions.

Let us now examine the characteristic waves of the periodic structure, including supports. For the vertical waves, the spectrum of attenuations, showing pass-bands and stop-bands (not drawn), is similar to the spectrum of Figure 5, although it includes an additional wave of high attenuation—a near-field wave—of little physical value. Thus we have confirmation that in this case the Timoshenko beam model and the kinematic model are equivalent. The wave vectors are also similar.

The "lateral wave" spectrum of computed attenuations is given in Figure 9. Here it can be seen that the results present a rather complex organization. One mode presents a high attenuation in the whole frequency range—a near field wave. Another mode also presents high attenuations beyond 1000 Hz, while the other two keep median values throughout the frequency range, with alternating stop-bands and pass-bands. Indeed, it is now not easy to label these different waves. Due to the considerable local influence of the supports, the waves do not have the simple organization which was found in continuous beam analysis, and can no longer be labelled using simple terms such as bending and torsion. Actually, the waves are uninterpretable "mixtures"—with complex coefficients—of the basic modes. Using the same normalizing rule as above, the wave composition is shown, in modulus, in Figure 10 for the 100 Hz frequency. Clearly, the interpretation of this graph is perplexing. In fact, such an interpretation is not very useful. The response of the structure to an excitation will be reconstructed from these characteristic waves in variable proportions, depending on the excitation shape. The most important question now is to know whether the set of characteristic waves allows a precise reconstruction of the track response or not.

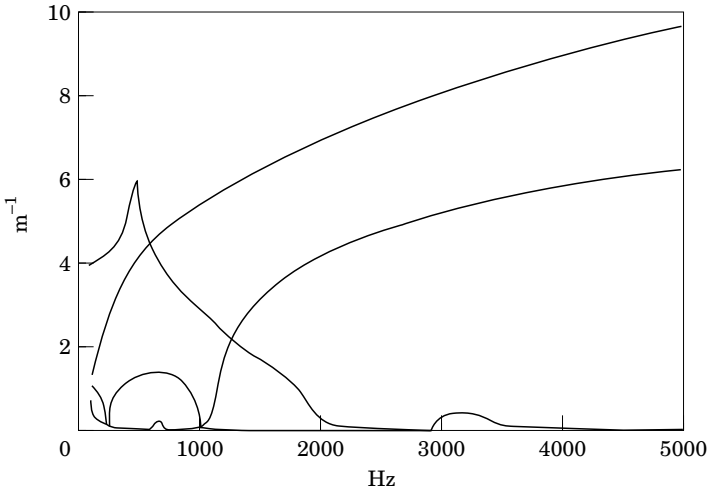


Figure 9. The attenuation factors of the lateral characteristic waves of the track: the case of a kinematic four-mode model.

### 4.6. EXPERIMENTAL VALIDATION AND ACCELERANCE RESULTS

From the same experimental data set, the computed accelerances can be compared with experimental measurements.

Let us consider the vertical and lateral accelerance plots. The excitation point is still at the head of the rail profile, first in a vertical direction and then in a lateral direction, on a cross-section in front of a support.

The reduced basis of displacements includes at least the global translational and rotational modes of the cross-section. The additional modes defined in section 4.1 will be incorporated later, and their influence will be appreciated through comparison with the experimental results.

Let us first consider the vertical receptance spectrum. A first computation is performed with the two rigid body modes involved in bending—a pure translation and a pure rotation. Therefore the transfer matrix is size 4. The computed spectrum (see Figure 11(a)),

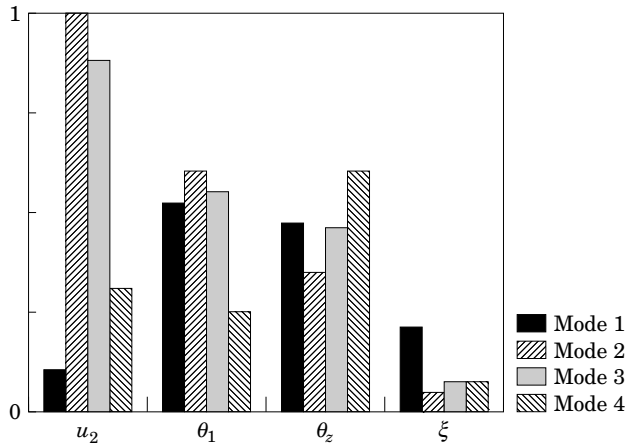


Figure 10. The relative compositions of the lateral characteristic waves of the track at 100 Hz.

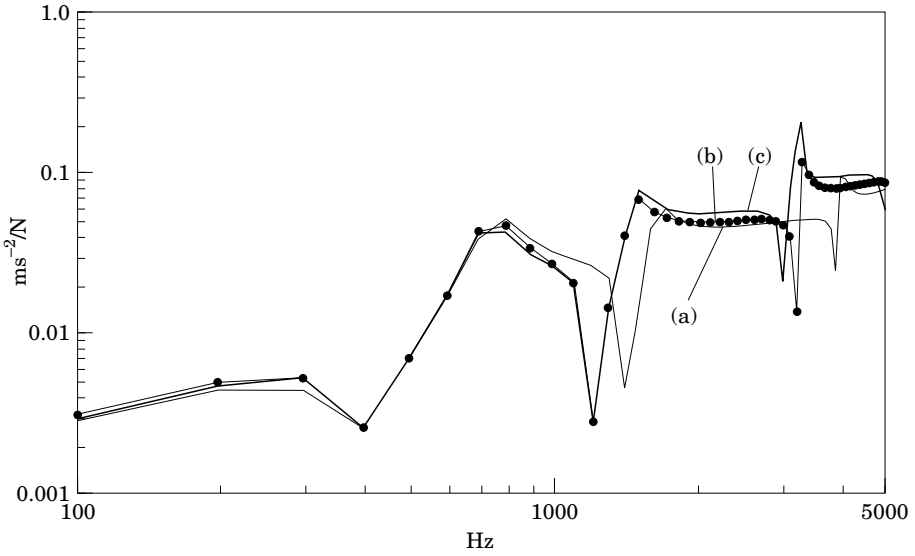


Figure 11. Vertical accelerance spectra: (a) the kinematic two-mode model; (b) Timoshenko model; (c) the kinematic three-mode model.

when compared with the Timoshenko spectrum (Figure 11(b)) or the experimental one (Figure 12(b)), exhibits a very similar shape: however, there is a global 100 Hz shift on the frequency axis. The model is roughly equivalent to an Euler–Bernouilli model.

It is expected that an appropriate cross-section mode related to shearing deformation could reduce this frequency gap. The shearing mode of section 4.1, obtained from a static F.E. analysis, is added to the reduced basis, resulting in a size 6 transfer matrix. The computed spectrum (Figure 11(c) or 12(a)), shows that the frequency shift has indeed

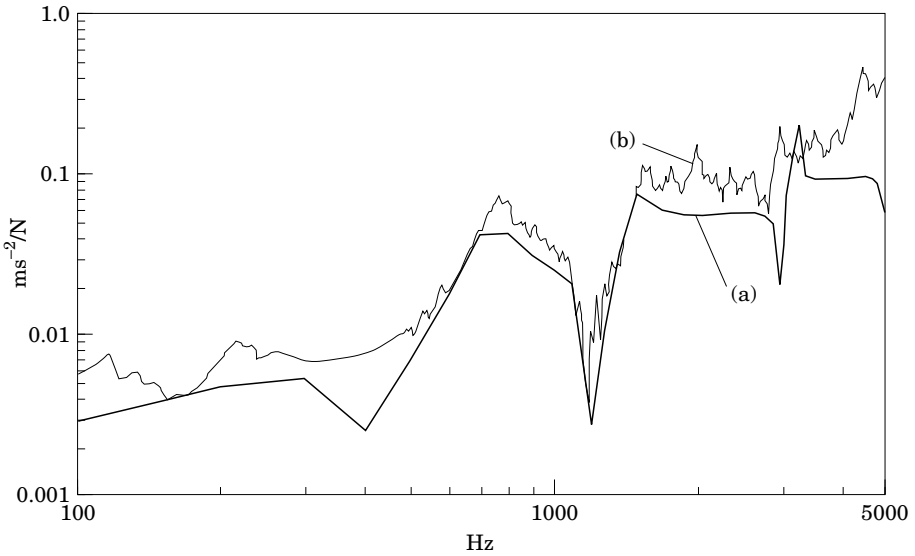


Figure 12. Further vertical accelerance spectra: (a) the kinematic three-mode model; (b) the experimental result.

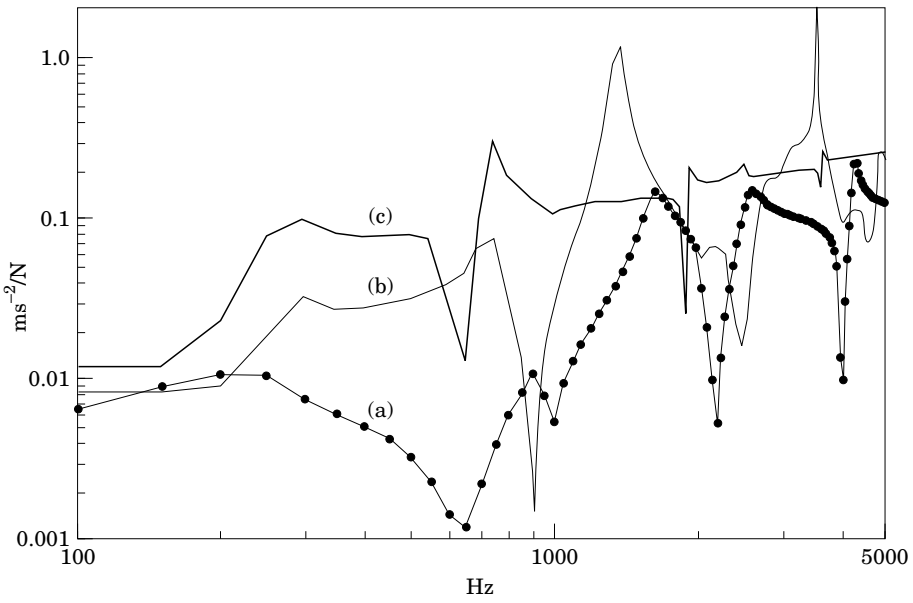


Figure 13. Computed lateral accelerance spectra: (a) the Timoshenko model; (b) the kinematic three-mode model; (c) the kinematic four-mode model.

disappeared, resulting in excellent agreement between the kinematic model and the Timoshenko model (Figure 11(b)), and satisfactory agreement with the experimental data. Therefore, at this point, the kinematic three-mode model is found to be strictly equivalent to the Timoshenko model, without resorting to the artifice of the Timoshenko factor correction.

Some differences compared with the experimental results remain in the lowest part of the spectrum, but can be easily explained by the fact that the dynamic characteristics of the supports are not well enough known. In the upper frequency range, the global level and the main spectrum features—the place of the pinned–pinned frequency, for instance—are found accurately. However, for frequencies above 1200 Hz, secondary peaks exist in the experimental spectrum, which are not given by the models. These peaks denote the existence of other modes that have not been included so far.

Now let us consider the lateral receptance spectrum. Here the main challenge remains to fill the large gap (10 dB) existing between the lateral receptance computed with the Timoshenko model (Figure 13(a)), and the experimental result (Figure 14(b)). At present time the model includes four rigid body modes $u_1$, $u_2$, $\theta_1$ and $\theta_2$, and the vertical shearing mode $\eta$. By taking into account the longitudinal rotation $\theta_3$, so that the transfer function is of size 12, a partial but insufficient improvement is obtained (Figure 13(b)). Clearly, the torsional phenomenon is not well represented by the pure rotation, since warping effects are allowed for in the present model.

The warping mode of section 4.1 is now added to the reduced basis (Figure 13(c)). The transfer matrix is thus of size 14. The general level of the computed spectrum comes close to the level of the experimental one, leading to very similar plots in the whole frequency range. Clearly, the additional modes have provided the necessary compliance that the beam needed to reach the proper deformation. It is striking to observe, but easy to understand from the physical point of view, that the whole deformation was severely blocked in the absence of the suitable degrees of freedom.

However, a difference still remains between the two spectra in the form of a global 100 Hz shift, as was found initially for the vertical receptance. Once more, it is expected that the trouble could be caused by the absence of the shearing compliance in lateral displacements. Therefore, in a manner similar to the vertical receptance, a lateral shearing mode is introduced into the model.

Unexpectedly, this task encounters specific numerical difficulties. Among the vibration modes generated by the free dynamic equations, one mode is found to have an attenuation factor in the $10^{13}$ range, resulting in such ill-conditioned equations that the following calculations break down.

Actually, this numerical difficulty is of great interest. Clearly, the problem can be attributed to the presence of near field waves of very short length. Moreover, it is to be expected that this problem will often be encountered when introducing further additional modes in the model. The reason is that, although these near field waves may be of little interest from the physical point of view, their existence is a mathematical necessity for completion of the displacement basis. For this reason, a general treatment of this situation must be looked for. Various ideas can be submitted to overcome the difficulty. One idea would be to express the dynamics on a reduced basis, the size of which would be less than the space dimension, so that near field waves could be ignored. Another idea would be to uncouple and treat separately the terms that contain the ill conditioned part of the transfer matrix. It is difficult to guess which method has the best chance of succeeding. An important theoretical effort has already been carried out in these directions. Despite very encouraging elements, satisfactory results are still not available. The outcome of these additional investigations will be reported in another paper.

Finally, by taking into account the inaccuracy of the data available for the supports, the data set used for computation can be adjusted slightly to improve the quality of the results. A physical argument for this operation could be that the support characteristics are dynamic rather than static, and so depend on the frequency. Two different data sets can thus be determined, one for the low frequency range and another for the high frequency range. The plot of Figure 14(a) was obtained in this way, showing a better agreement with the experimental data.

A similar analysis could have been performed for any locus of the excitation point; for instance, at mid-span. In Figure 15 are shown the results for a lateral excitation at this point, again at the top of the cross-section. The mechanical data set is the same as above and computation includes the four lateral modes. Results are presented in Figure 15(a).

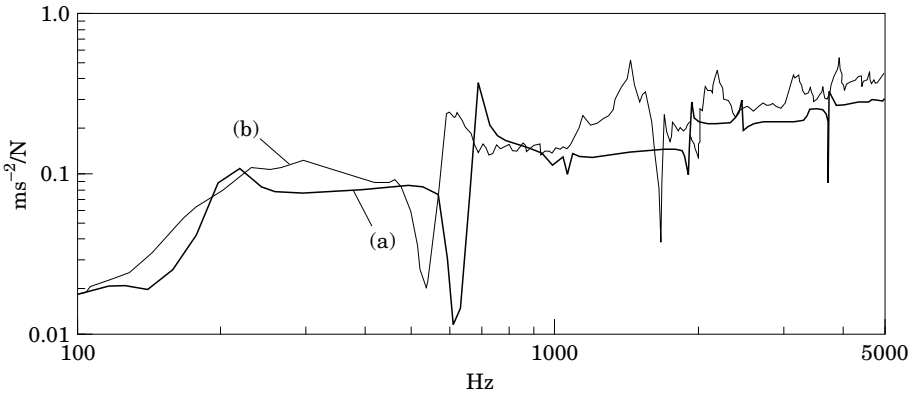


Figure 14. Further lateral accelerance spectra: (a) the kinematic four-mode model with data set adjustment; (b) the experimental result.

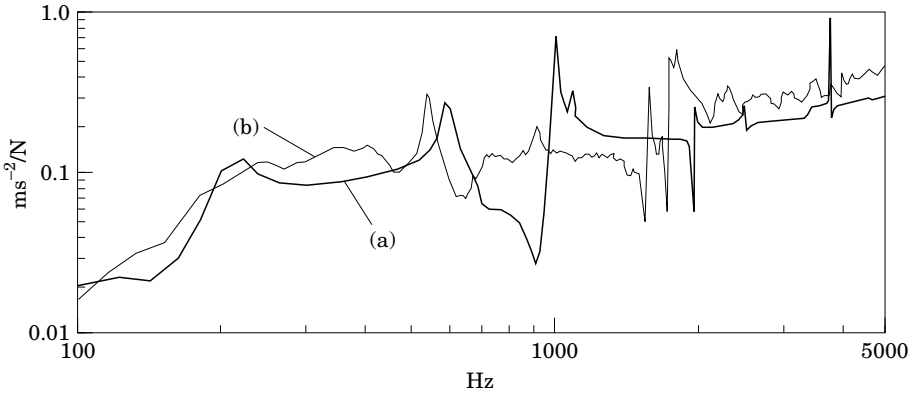


Figure 15. Lateral accelerance spectra for an excitation at mid-span: (a) kinematic four-mode model; (b) the experimental result.

Again, the results can be compared with Figure 15(b), obtained from experimental measurements, leading to the same conclusion as above.

## 5. CONCLUSIONS

Modelling railway track vibration can be a very powerful tool in view of reducing rail traffic noise. In the present paper the insufficiency of the classical beam models was emphasized, leading to the conclusion that a model taking into account some refined deformation modes of the cross-section would be more appropriate.

In the second half of the paper, it was clearly shown that a dramatic improvement of the results could be expected from an enriched kinematic approach. For instance, in the vertical direction, the computed and experimental receptance spectra were brought very close together by adding only one additional mode to the classical rigid body modes of translation and rotation. This mode accounts for the shearing deformation and its presence is equivalent to the Timoshenko factor. In the lateral direction, a global 10 dB gap between the two spectra could be overcome through the incorporation of a torsional mode, and a quite satisfactory agreement between the two curves could be reached through a slight adjustment of the support characteristics, here considered to be frequency dependent.

Despite these very encouraging results, some localized discrepancies remain, which will have to be dealt with in the future. For instance, the experimental spectrum exhibits high frequency peaks which do not appear in the computed spectrum, indicating that more modes, or perhaps span modes, have to be introduced into the model. In addition, a remaining 50 Hz gap between the computed and measured lateral spectra confirms an excessive general stiffness of the model, leading to the same conclusion.

In fact, the above investigations have shown that the introduction of such additional modes, due to the presence of near field waves, could result in serious numerical difficulties. Therefore a general investigation of this problem is looked upon as an essential step on the way to further developments.

The next challenge now lies in an accurate representation of high frequency modes. The problem is to determine and select the useful cross-section modes to include in the model. A study of the free propagating waves in the rail could provide a solution. The treatment of numerical problems could also be decisive. The theoretical difficulties are now identified but, ultimately, the results will have to be checked against experimental data. This is a necessary validation, and it is the only true validation.

## ACKNOWLEDGMENTS

This work was supported by the S.N.C.F., with Dr Pierre Etienne Gautier and Mr Paul Caille as contract monitors. The authors also gratefully acknowledge the help of Dr Didier Clouteau.

## REFERENCES

1. P. J. Remington 1976 *Journal of Sound and Vibration* **46**, 359–380. Wheel/rail noise, Part I: characterization of the wheel/rail dynamic system.
2. S. L. Grassie, R. W. Gregory, D. Harrison and K. L. Johnson 1982 *Journal of Mechanical Engineering Science* **24**, 77–95. The dynamic response of railway track to high frequency vertical excitation.
3. D. J. Thompson 1992 *Doctoral Thesis*, *University of Southampton*. Wheel–rail noise: theoretical modelling of the generation of vibrations.
4. L. Brillouin 1946 *Wave Propagation in Periodic Structures*. New York: Dover.
5. D. J. Mead and S. Markus 1983 *Journal of Sound and Vibration* **90**, 1–24. Coupled flexural–longitudinal wave-motion in a periodic beam.
6. D. J. Mead 1986 *Journal of Sound and Vibration* **104**, 9–27. A new method of analyzing wave propagation in periodic structures; applications to periodic Timoshenko beams and stiffened plates.
7. R. M. Orris and M. Petyt *Journal of Sound and Vibration* **33**, 223–236. A finite element study of harmonic wave propagation in periodic structures.
8. D. J. Mead 1975 *Journal of Sound and Vibration* **40**, 19–39. Wave propagation and natural modes in periodic systems: II. Multi-coupled systems, with and without damping.
9. J. Signorelli and A. H. Von Flotow 1988 *Journal of Sound and Vibration* **126**, 127–144. Wave propagation, power flow and resonance in a truss beam.
10. W. J. Chen and C. Pierre 1991 *Proceedings of the* 32*nd American Institute of Aeronautics and Astronautics*, *Structural Dynamics Conference*, Baltimore, U.S.A. Exact linear dynamics of periodic and disordered truss beams: localization of normal modes and harmonic waves.
11. W. J. Chen and C. Pierre 1992 *Proceedings of the* 33*rd Americal Institute of Aeronautics and Astronautics*, *Structural Dynamics Conference*, *Dallas*, *U.S.A*. Vibration localization and wave conversion phenomena in multi-coupled, nearly periodic, disordered truss beam.
12. D. J. Mead 1970 *Journal of Sound and Vibration* **11**, 181–197. Free wave propagation in periodically supported infinite beams.
13. D. J. Mead and Y. Yaman 1990 *Journal of Sound and Vibration* **141**, 465–484. The harmonic response of uniform beams on multiple linear supports: a flexural wave analysis.
14. D. J. Mead 1973 *Journal of Sound and Vibration* **27**, 235–260. A general theory of harmonic wave propagation in linear periodic systems with multiple coupling.
15. D. J. Mead 1975 *Journal of Sound and Vibration* **40**, 1–18. Wave propagation and natural modes in periodic systems: I. Mono-coupled systems.
16. C. Pierre 1988 *Journal of Sound and Vibration* **126**, 485–502. Mode localization and eigenvalue loci veering phenomena in disordered structures.
17. C. Pierre 1990 *Journal of Sound and Vibration* **139**, 111–132. Weak and strong vibration localization in disordered structures: a statistical investigation.
18. J. F. Doyle 1989 *Wave Propagation in Structures*. New York: Springer–Verlag.
19. M. Heckl 1992 *Report to the ORE Committee C* 163. Theoretical predictions for the acoustic behaviour of five types of European railway track.

## APPENDIX A: RECEPTANCE MATRIX AT A POINT OF THE RAIL

The receptance matrix is developed under the assumption that the applied force and the response signals are captured at the same point $P$ of the rail, in the same direction (see Figure A1).

The measured displacement $\mathbf{u}$ at a point P of the rail is related to the generalized displacements $\mathbf{u}_s$ of the cross-section $S_P$ of this point by the equation

$$\mathbf{u} = \mathbf{D}\mathbf{u}_s. \tag{A1}$$

This relation can be easily derived from the definition of the generalized displacements. Similarly, the applied force $\mathbf{F}$ at the same point $P$ is related to the generalized forces $\mathbf{f}_s$ applied on the cross-section $S_P$ by the relation:

$$\mathbf{f}_s = \mathbf{D}^{\mathrm{T}}\mathbf{F}, \tag{A2}$$

which is derived from equation (39) and the virtual work expression.

An elementary beam slice being defined around $P$ (see Figure A1), this slice is submitted to the forces $-\mathbf{f}_L$ and $\mathbf{f}_R$ on its faces, so that for equilibrium we have

$$\mathbf{f}_s - \mathbf{f}_L + \mathbf{f}_R = \mathbf{0}. \tag{A3}$$

The forces $\mathbf{f}_L$ and $\mathbf{f}_R$ can be expressed by using the impedance matrices of the left- and right-hand parts of the span. These matrices have the same form as in equation (5), except that the impedance $\mathbf{H}/2$ appears in one line only, because only one side of the beam part is concerned with the support reaction. Indexes $L$ and $R$ are used to indicate which part of the beam is referenced, left or right. From the corresponding impedance equations, the following expressions are easily derived:

$$\mathbf{f}_L = \mathbf{Z}^L_{21}\mathbf{u}_{n-1} + \mathbf{Z}^L_{22}\mathbf{u}_s, \qquad \mathbf{f}_R = -\mathbf{Z}^R_{11}\mathbf{u}_s - \mathbf{Z}^R_{12}\mathbf{u}_n, \tag{A4}$$

$$\mathbf{f}_{n-1} = -(\mathbf{Z}^L_{11} + \mathbf{H}/2)\mathbf{u}_{n-1} - \mathbf{Z}^L_{12}\mathbf{u}_s, \qquad \mathbf{f}_n = \mathbf{Z}^R_{21}\mathbf{u}_s + (\mathbf{Z}^R_{22} + \mathbf{H}/2)\mathbf{u}_n, \tag{A5}$$

where $\mathbf{u}_s$ denotes for the displacement vector of section $S_p$.

The submatrices $\mathbf{Z}^L_{ij}$ and $\mathbf{Z}^R_{ij}$ are drawn from the left and right transfer matrices $\mathbf{Z}^L$ and $\mathbf{Z}^R$, which are built in the same way as the whole span transfer matrix $\mathbf{Z}$.

As no external force is applied on the left-hand face of cross-section $S_p$, the wave system on this side can be assumed to be a sum of left propagating waves, so that equations (14) and (15) reduce to

$$\mathbf{u}_{n-1} = \beta_i \boldsymbol{\varphi}^L_i, \qquad \mathbf{f}_{n-1} = -\beta_i \mathbf{g}^L_i, \tag{A6}$$

and, similarly, on the right-hand side of $S$,

$$\mathbf{u}_n = \alpha_i \boldsymbol{\varphi}^R_i, \qquad \mathbf{f}_n = -\alpha_i \mathbf{g}^R_i. \tag{A7}$$

From the system of nine equations (A3)–(A7), the six vectors $\mathbf{u}_{n-1}$, $\mathbf{u}_n$, $\mathbf{f}_{n-1}$, $\mathbf{f}_n$, $\mathbf{f}_L$ and $\mathbf{f}_R$ can be easily eliminated. Upon gathering the column vectors $\boldsymbol{\varphi}^L_i$, $\boldsymbol{\varphi}^R_i$, $\mathbf{g}^L_i$, $\mathbf{g}^R_i$ into matrices

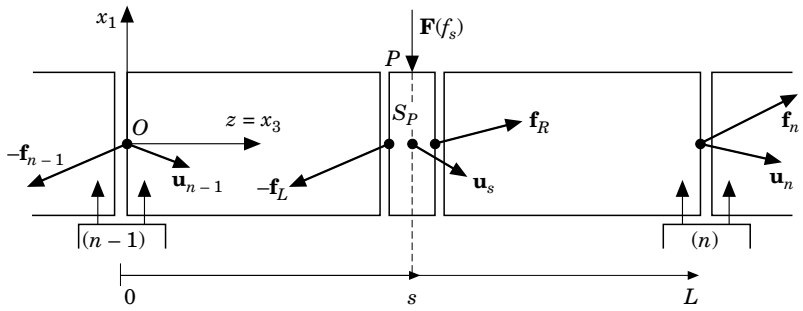


Figure A1. A receptance computation: the definition of forces and displacements.

$\boldsymbol{\varphi}^L$, $\boldsymbol{\varphi}^R$, $\mathbf{g}^L$ and $\mathbf{g}^R$, and the coefficients $\alpha_i$ and $\beta_i$ into the vectors $\boldsymbol{\alpha}$ and $\boldsymbol{\beta}$, the three remaining equations take the form

$$[\mathbf{g}^R + (\mathbf{Z}^R_{22} + \mathbf{H}/2)\boldsymbol{\varphi}^R]\boldsymbol{\alpha} + \mathbf{Z}^R_{21}\mathbf{u}_s = \mathbf{0},$$

$$[\mathbf{g}^L + (\mathbf{Z}^L_{11} + \mathbf{H}/2)\boldsymbol{\varphi}^L]\boldsymbol{\beta} + \mathbf{Z}^L_{12}\mathbf{u}_s = \mathbf{0}, \tag{A8}$$

$$\mathbf{Z}^R_{12}\boldsymbol{\varphi}^R\boldsymbol{\alpha} + \mathbf{Z}^L_{21}\boldsymbol{\varphi}^L\boldsymbol{\beta} + (\mathbf{Z}^R_{11} + \mathbf{Z}^L_{22})\mathbf{u}_s = \mathbf{f}. \tag{A9}$$

Then the vectors $\boldsymbol{\alpha}$ and $\boldsymbol{\beta}$ can be extracted from equation (46), so that the impedance formulae result from equation (47):

$$\boldsymbol{\alpha} = \mathbf{h}^R\mathbf{u}_s, \qquad \boldsymbol{\beta} = \mathbf{h}^L\mathbf{u}_s, \qquad \mathbf{u}_s = \mathbf{W}_s^{-1}\mathbf{f}_s, \tag{A10}$$

with

$$\mathbf{h}^R = -[\mathbf{g}^R + (\mathbf{Z}^R_{22} + \mathbf{H}/2)\boldsymbol{\varphi}^R]^{-1}\mathbf{Z}^R_{21},$$

$$\mathbf{h}^L = -[\mathbf{g}^L + (\mathbf{Z}^L_{11} + \mathbf{H}/2)\boldsymbol{\varphi}^L]^{-1}\mathbf{Z}^L_{12},$$

$$\mathbf{W}_s = \mathbf{Z}^R_{11} + \mathbf{Z}^L_{22} + \mathbf{Z}^R_{12}\boldsymbol{\varphi}^R\mathbf{h}^R + \mathbf{Z}^L_{21}\boldsymbol{\varphi}^L\mathbf{h}^L. \tag{A11}$$

From equation (A1) and (A2), the receptance equation becomes

$$\mathbf{u} = \mathbf{D}\mathbf{W}_s^{-1}\mathbf{D}^{\mathrm{T}}\mathbf{F}, \tag{A12}$$

which defines the receptance matrix at point $P$ for a load at the same point:

$$\mathbf{H}_{PP} = \mathbf{D}\mathbf{W}_s^{-1}\mathbf{D}^{\mathrm{T}}.$$

## APPENDIX B: IMPEDANCE MATRICES FOR THE EULER–BERNOUILLI AND TIMOSHENKO BEAMS

In the method, one considers separately the effects of vertical motion, lateral motion—including both bending and shearing effects—and torsion.

The equations of free vertical motion are

$$EI_1\,\partial^4 u_1/\partial z^4 - \rho S\ddot{u}_1 = 0, \qquad \theta_2 = \partial u_1/\partial z, \qquad T_1 = EI_1\,\partial^3 u_1/\partial z^3,$$

$$M_2 = -EI_1\,\partial^2 u_1/\partial z^3 \tag{B1}$$

for the Euler–Bernouilli model, and

$$GSK_1\,\partial^2 u_1/\partial z^2 + GSK_2\,\partial\theta_2/\partial z + \rho S\ddot{u}_1 = 0,$$

$$EI_1\,\partial^2\theta_2/\partial z^2 - GSK_1\,\partial u_1/\partial z - GSK_1\theta_2 + \rho\omega^2 I_1\ddot{\theta}_2 = 0,$$

$$T_1 = GSK_1(\partial u_1/\partial z + \theta_2), \qquad M_2 = EI_1\,\partial\theta_2/\partial z \tag{B2}$$

for the Timoshenko model.

In these equations, $S$ and $I_1$ are the area and the vertical inertia of the cross-section, $K_1$ is the corresponding Timoshenko factor, $T_1$ and $M_2$ are the current shearing force and bending moment under vertical bending, $E$, $G$ are the Young's and shear modulus, and $\rho$ is the mass per unit volume of the material.

The procedure to obtain the impedance matrix is similar in both cases. It involves the following sequence, which can be easily programmed on a computer.

(1) Take the Fourier transform of the equations, just replacing $\ddot{X}$ by $\omega^2 X$.

(2) Look for an exponential solution, defining a characteristic wave: $u_1 = A\exp(rz)$, $\theta_2 = B\exp(rz)$. In the Euler–Bernouilli case, the second equation is a consequence of the first one. This step results in a set of homogeneous equations for $A$ and $B$. The

compatibility of these equations is ensured with four characteristic values of $r$: two real values and two pure imaginary values.

(3) Look for solutions of the actual problem in the space of characteristic waves:

$$u_1 = A_1 \exp(r_1 z) + A_2 \exp(r_2 z) + A_3 \exp(r_3 z) + A_4 \exp(r_4 z),$$

$$\theta_2 = B_1 \exp(r_1 z) + B_2 \exp(r_2 z) + B_3 \exp(r_3 z) + B_4 \exp(r_4 z).$$

This means that the coefficients $A_i$ and $B_i$ must be determined so as to fulfil the end conditions:

$$u_1(0) = u_0^1, \qquad u_1(L) = u_L^1, \qquad \theta_2(0) = \theta_0^2, \qquad \theta_2(L) = \theta_L^2,$$

$$T_1(0) = T_0^1, \qquad T_1(L) = T_L^1, \qquad M_2(0) = M_0^2, \qquad M_2(L) = M_L^2.$$

(4) From the above procedure, a relation is found between the vectors of end displacements and end forces:

$$\mathbf{U}^1 = [u_0^1 \quad \theta_0^2 \quad u_L^1 \quad \theta_L^2]^{\mathrm{T}}, \qquad \mathbf{F}^1 = [-T_0^1 \quad -M_0^2 \quad T_L^1 \quad M_L^2]^{\mathrm{T}}, \qquad \mathbf{F}^1 = \mathbf{Z}_{11}\mathbf{U}^1.$$

The matrix $\mathbf{Z}_{11}$, of size $4 \times 4$ is part of the impedance matrix.

The lateral motion is analyzed in a similar way and provides a matrix $\mathbf{Z}_{22}$ which is part of the impedance matrix.

The equations of motion in torsion are

$$G\,\partial^2\theta_z/\partial z^2 + \rho\ddot{\theta}_z = 0, \qquad M_z = G(I_1 + I_2)\partial\theta_z/\partial z. \tag{B3}$$

The development of the partial impedance matrix due to torsion is similar, except that the characteristic waves have only two terms. An impedance matrix $\mathbf{Z}_{33}$ of size $2 \times 2$ is found.

Finally, assembling the impedance equations into one, and then rearranging the lines and columns so as to gather the left end variables into one group and the right end variables into another group, the global impedance matrix of size $10 \times 10$ is found.